AVERAGE AMPLIFICATION FACTOR OF SH WAVES IN IRREGULARLY LAYERED MEDIA

Hidenori MOGI[1] And Hideji KAWAKAMI[2]

SUMMARY

The effects of subsurface irregularities on the amplification characteristics have been widely recognized as an important factor. However, the various studies based on numerical analysis have shown the variability of the response against the incident wave field. To estimate the expected amplification effects of subsurface irregularities without any consideration of the seismic source, the average amplification factor has been introduced. Further, to demonstrate the validity of the average amplification factor, it has been applied to the ground model of Kobe City and compared with the amplification factors due to one-dimensional multiple reflections and a plane wave incident. From these results, it has been concluded that the average amplification factor can represent a measure of amplification effects of subsurface irregularities in the case when the incident wave field is unpredictable.

INTRODUCTION

The effects of subsurface irregularities on the amplification characteristics have been widely recognized as an important factor. To illustrate this effect, various studies based on numerical analyses such as the boundary element method have been performed. These results show us the complexity of the surface response and its variability against the incident wave field. Considering these phenomena, if the incident waves are predictable with some degree of precision, the surface response can be estimated by using numerical analyses. However, due to difficulties in predicting a faulting process, these analyses are valid for few cases.

From this point of view, we have introduced the average amplification factor to estimate the expected amplification effects of subsurface irregularities without any consideration of the seismic source. The average amplification factor has been defined as the ratio of the average spectral amplitude of surface motion to that of incident waves at the bedrock boundary. The average spectral amplitude of incident waves at the interface has been formulated under a stochastic assumption that the incident wave field consists of plane waves in all directions with random and mutually independent amplitudes. Transfer functions from the interface to a ground surface have been estimated from the boundary element method.

To demonstrate the validity of the average amplification factor, the ground model of Kobe City has been used. For the purpose of comparison, both the one-dimensional amplification factor based on the multiple reflection theory and the amplification factor to an incident plane wave have also been estimated. The comparisons have been made both in a frequency axis with fixed surface locations and in a space axis with fixed frequencies.

These comparisons have shown that the plane wave amplification factors have variability against the changes of the incident angles, observational locations and frequencies. On the contrary, the average amplification shows stability against those changes and has the shape approximately consistent with the envelope of the plane wave amplification factors. From these results, it has been concluded that the average amplification factor can represent a measure of amplification effects of subsurface irregularities in the case when the incident wave field is unpredictable.

[1] *Dept of Civil & Environmental Engineering, Saitama University, Urawa, Japan. E-mail hmogi@kiban.civil.saitama-u.ac.jp*
[2] *Dept of Civil & Environmental Engineering, Saitama University, Urawa, Japan. E-mail kaw@kiban.civil.saitama-u.ac.jp*

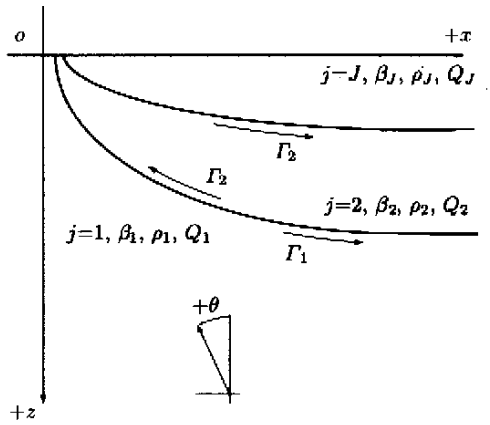

Figure 1: Two-dimensional coordinate system

2. BOUNDARY ELEMENT METHOD

2.1 BOUNDARY INTEGRAL EQUATION

We consider a two-dimensional ground model consisting of J elastic layers as shown in Fig.1. Displacements of SH waves with time harmonic dependence satisfy the Helmhortz equation

$$\left\{\nabla^2 + k_{\beta_j}^2\right\} u_j(X;\omega) = 0\,, \qquad j = 1, 2, \ldots, J, \tag{1}$$

where $u_j(X;\omega)$ is a displacement at arbitrary point $X = (x, z)$ in the j-th layer, ω is the circular frequency, β_j is the shear wave velocity and k_{β_j} is the wave-number of the S wave given by $k_{\beta_j} = \omega/\beta_j$.

From Eq.(1), the following integral equation can be obtained,

$$\frac{1}{2}u_j(X) + v.p.\int_{\Gamma_j} q_j^*(Y,X)\,u_j(Y)\,d\Gamma(Y) - \int_{\Gamma_j} u_j^*(Y,X)\,q_j(Y)\,d\Gamma(Y) = \begin{cases} v(X) & (j=1) \\ 0 & (j \geq 2) \end{cases} \tag{2}$$

where X and Y are points on the boundary Γ_j, $v.p.$ indicates a Cauchy principal-value integral, $v(x)$ is the dispacement of the incident wave, and $q(X)$ is a gradient of $u(X)$ in normal direction n. The fundamental solutions $u^*(Y,X)$ and $q^*(Y,X)$ are given by

$$\begin{aligned} u_j^*(Y,X) &= -\frac{i}{4}H_0^{(2)}(k_{\beta_j} r) \\ q_j^*(Y,X) &= \frac{\partial u_j^*(Y,X)}{\partial n(Y)} = \frac{ik_{\beta_j}}{4}H_1^{(2)}(k_{\beta_j} r)\frac{\partial r}{\partial n(Y)}, \end{aligned} \tag{3}$$

where r is the distance between X and Y, and $H_\nu^{(2)}(\cdot)$ is the Hankel function of the second kind of order ν[Brebbia and Walker, 1980].

2.2 DISCRETIZATION OF BOUNDARY INTEGRAL EQUATION

For the numerical solution of the boundary integral equations (2), the boundaries $\Gamma_j, (j = 1, \ldots, J)$ are divided into N_j elements $\Gamma_{jk}, (k = 1, \ldots, N_j)$. We assume that $u(Y)$ and $q(Y)$ are piecewisely constant on the boundaries, which can be expressed as nodal boundary values

$$\boldsymbol{u}_j(X) = \{u_j(X_1), \ldots, u_j(X_{N_j})\}^T\,, \quad \boldsymbol{q}_j(X) = \{q_j(X_1), \ldots, q_j(X_{N_j})\}^T, \tag{4}$$

where X_k is the midpoint of the boundary element Γ_{jk}. Using the nodal values, the boundary integral equations (2) can be discretized as

$$\frac{1}{2}u_j(X_{k'}) + \sum_k u_j(Y_k)\int_{\Gamma_{jk}} q_j^*(Y,X_{k'})\,d\Gamma(Y) - \sum_k q_j(Y_k)\int_{\Gamma_{jk}} u_j^*(Y,X_{k'})\,d\Gamma(Y) = \begin{cases} v(X_{k'}) & (j=1) \\ 0 & (j \geq 2). \end{cases} \tag{5}$$

Eq.(5) can be written in following simultaneous equations

$$\boldsymbol{H}_j \boldsymbol{u}_j - \boldsymbol{G}_j \boldsymbol{q}_j = \begin{cases} \boldsymbol{v} & (j=1) \\ \boldsymbol{0} & (j \geq 2) \end{cases} \tag{6}$$

where the coefficient matrices $\boldsymbol{H}$ and $\boldsymbol{G}$ are from integration in Eq.(5). A twelve-point Gaussian numerical quadrature was used for computing the components of the matrices except for the diagnoal ones. The diagonal components of $\boldsymbol{H}$ vanish due to the term $\partial r/\partial n(Y)$ in Eq.(3), and for $\boldsymbol{G}$ it was analytically determined after expanding in series.

2.3 BOUNDARY ELEMENT MATRIX FOR LAYERED MEDIA

Let the k-th node in j-th layer and k'-th node in j'-th layer are in contact. Continuity conditions that ought to be satisfied across the interfaces for displacements and shear stresses respectively, are

$$u_{jk}=u_{j'k'}\ ,\quad T_{jk}=-T_{j'k'} \tag{7}$$

where u_{jk} is the abbreviation for $u_j(X_k)$, and T_{jk} is the shear stress given by $T_{jk} = \mu_j\, q_j(X_k)$. By using Eq.(7), Eq.(6) can be expressed as

$$\boldsymbol{A} \left\{ \begin{array}{c} \boldsymbol{u} \\ \boldsymbol{T} \end{array} \right\} = \left\{ \begin{array}{c} \boldsymbol{v} \\ \boldsymbol{0} \end{array} \right\} \tag{8}$$

where the matrix $\boldsymbol{A}$ is an assembly of $\boldsymbol{H}_j$ and $\boldsymbol{G}_j/\mu_j$ for all j.

3. AVERAGE AMPLIFICATION FACTOR FOR THE GROUND WITH IRREGULAR SUBSURFACE TOPOGRAPHY

3.1 RESPONSE FUNCTION

To derive the response functions of the ground, the inverse relation of Eq.(8) is used.

$$\left\{ \begin{array}{c} \boldsymbol{u} \\ \boldsymbol{T} \end{array} \right\} = \boldsymbol{A}^{-1} \left\{ \begin{array}{c} \boldsymbol{v} \\ \boldsymbol{0} \end{array} \right\} \tag{9}$$

From Eq.(9), the displacement of the k-th node (assumed to be a surface node here), can be expressed as

$$u_k = \{p_{k1}, \ldots, p_{kn}, \ldots, p_{kN}\} \{v_1, \ldots, v_n, \ldots, v_N\}^T \equiv \boldsymbol{p}_k \boldsymbol{v} \tag{10}$$

where $p_{kn}, (n = 1, \ldots, N)$ are coefficients of the displacements of incident wave $v_n, (n = 1, \ldots, N)$, taken from the k-th row of the matrix $\boldsymbol{A}^{-1}$. The coefficient p_{kn} corresponds to the response function of the k-th node to the displacement of the incident wave at the n-th node, including the multiple reflection effects.

3.2 AVERAGED AMPLIFICATION FACTOR

Using Eq.(10), the power spectrum at the k-th node can be expressed as

$$S_k = u_k u_k^* = \boldsymbol{p}_k \boldsymbol{V} \boldsymbol{p}_k^H \tag{11}$$

where * and ^{H} indicate the complex conjugate and conjugate transpose respectively. $\boldsymbol{V}$ is the matrix of cross-spectrum of the incident wave at the bedrock-deposite interface, defined by

$$\boldsymbol{V} = \boldsymbol{v}\boldsymbol{v}^H = \begin{bmatrix} S^I_{11} & \cdots & S^I_{1N} \\ \vdots & \ddots & \vdots \\ S^I_{N1} & \cdots & S^I_{NN} \end{bmatrix} \tag{12}$$

where ^{I} indicates quantities of the incident wave.

Next, the displacement of the incident wave v_n is expressed as a superposition of plane waves with various incident angles,

$$v_n = \sum_{\ell=1}^{K} a_\ell \exp(i\,\xi_\ell x_n + i\,\gamma_\ell z_n) \tag{13}$$

where ξ_ℓ and γ_ℓ, $(\ell = 1, \ldots, K)$ are the wave-numbers in the x- and z-directions, respectively. Using the incident angle θ_ℓ, these wave-numbers can be given by

$$\xi_\ell = k_{\beta_1} \sin\theta_\ell \ , \quad \gamma_\ell = k_{\beta_1} \cos\theta_\ell . \tag{14}$$

In this study, θ_ℓ are assumed to be at equal intervals in the range of $-\pi/2$ to $\pi/2$.

The complex amplitudes a_ℓ are assumed to be zero-mean and mutually independent random variables:

$$\mathrm{E}(a_\ell) = 0 \ , \quad \mathrm{E}(a_\ell a_{\ell'}^*) = \begin{cases} \alpha & (\ell = \ell') \\ 0 & (\ell \neq \ell') \end{cases} \ , \qquad \ell, \ell' = 1, \ldots, K \tag{15}$$

where the variance α is assumed to be identical for all incident angles θ_ℓ. The cross-spectrum between the displacements of the incident wave at the n-th and n'-th nodes can be expressed as

$$S_{nn'}^I = v_n v_{n'}^* = \boldsymbol{e}_n \boldsymbol{a}\boldsymbol{a}^H \boldsymbol{e}_{n'}^H = \boldsymbol{e}_n \begin{bmatrix} a_1 a_1^* & \cdots & a_1 a_K^* \\ \vdots & \ddots & \vdots \\ a_K a_1^* & \cdots & a_K a_K^* \end{bmatrix} \boldsymbol{e}_{n'}^H \tag{16}$$

where $\boldsymbol{e}_n$ and $\boldsymbol{a}$ are respectively K-dimensional row and column vectors given by

$$\boldsymbol{e}_n = \{\exp(i\xi_1 x_n + i\gamma_1 z_n), \ldots, \exp(i\xi_\ell x_n + i\gamma_\ell z_n), \ldots, \exp(i\xi_K x_n + i\gamma_K z_n)\} \tag{17}$$

$$\boldsymbol{a} = \{a_1, \ldots, a_\ell, \ldots, a_K\}^T . \tag{18}$$

The components of the matrix $\boldsymbol{a}\boldsymbol{a}^H$ will vanish by averaging except the diagonal ones because of the properties shown in Eq.(15). The average cross-spectrum can be given by

$$\mathrm{E}\left(S_{nn'}^I\right) = \mathrm{E}\left(v_n v_{n'}^*\right) = \alpha \sum_{\ell=1}^{K} \exp\{i\,\xi_\ell (x_n - x_{n'}) + i\,\gamma_\ell (z_n - z_{n'})\}, \quad n, n' = 1, \ldots, N \ . \tag{19}$$

Substituting $n' = n$ into Eq.(19), we get

$$\mathrm{E}(S_{nn}^I) = K\alpha, \quad n = 1, \ldots, N, \tag{20}$$

the power spectra of the incident wave become identical in the sense of average.

Averaging Eq.(11) and using Eqs (16) to (20), the relationship between the average power spectra at the surface and those of incident wave at the bedrock-deposit interface can be derived as

$$\mathrm{E}(S_k) = \mathrm{E}(S_{nn}^I)\ R_k^2 \tag{21}$$

where

$$R_k^2 = \boldsymbol{p}_k \begin{bmatrix} E_{11} & \cdots & E_{1N} \\ \vdots & \ddots & \vdots \\ E_{N1} & \cdots & E_{NN} \end{bmatrix} \boldsymbol{p}_k^H \tag{22}$$

$$E_{nn'} = \frac{1}{K} \sum_{\ell=1}^{K} \exp\{i\xi_\ell (x_n - x_{n'}) + i\gamma_\ell (z_n - z_{n'})\} \ . \tag{23}$$

Since the coefficient R_k in Eq.(21) gives a measure of amplification in the sense of average, we will call this as the average amplification factor here. Also from Eqs (19), (20) and (23), the following relationship can be found:

$$\mathrm{E}\left(S_{nn'}^I\right) = \mathrm{E}\left(S_{nn}^I\right)\ E_{nn'} \ . \tag{24}$$

As shown in Eq.(24), $E_{nn'}$ corresponds to the coherence function of the incident wave, and will be called as the average coherence function here.

It is worth mentioning that the surface response is affected by the coherence of the incident wave field as well as the response function, because V in Eq.(11) depends on the coherence. Further, as Eq.(23) shows, this effect is that the large values of the average coherence magnify the changes of the response function in the surface response. Considering that the response function depends on the frequency and the observational location, it can be understood that the their changes will strongly vary the surface response against the high-coherent incident wave field.

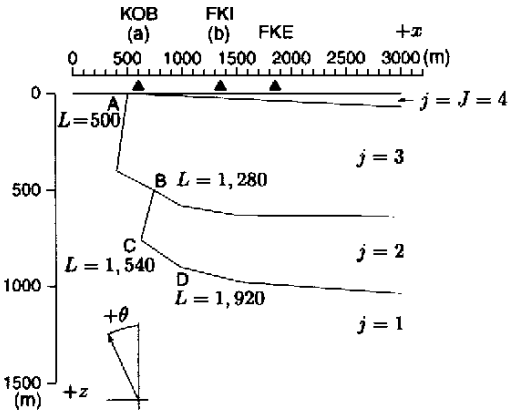

Figure 2: Two-dimensional ground model of Higashi-Nada ward, Kobe

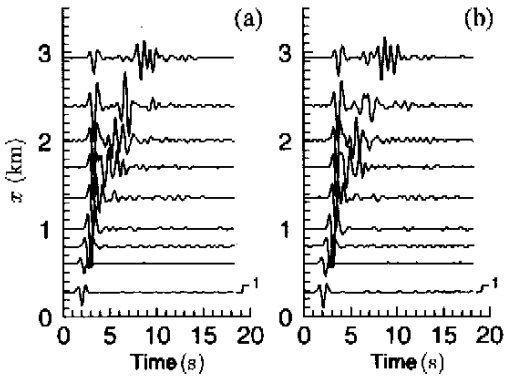

Figure 3: Displacements at the ground surface due to Ricker-wavelet (f_p = 1Hz) with 0°(a) and 20°(b) incident angles

4. NUMERICAL ANALYSIS USING KOBE GROUND MODEL

4.1 GROUND MODEL AND BOUNDARY ELEMENT ANALYSIS

To demonstrate the validity of the average amplification factor, the ground model of Kobe City shown by Fig.2 has been used. This model is based on the model developed by Pitarka[Pitarka *et al.*, 1996] to investigate the amplification characteristics based on numerical analyses and the seismograms observed during the aftershocks of the 1995, Hyogo-ken Nanbu Earthquake. And this model had been partially changed to reduce computational efforts.

The physical properties of the ground are tabulated in Tab.1. The Q-values have been taken from the one-dimensional ground model at the FKE site[Iwata *et al.*, 1996].

Array observations had been made at the several points including the KOB, FKI and FKE sites[Irikura, 1995; Iwata *et al.*, 1996]. The FKI site is located in the severely damaged band, and the KOB and FKI sites are in the vicinity of the northern and southern edges of the damaged band respectively. In their study, the characteristics of the ground motion have been revealed from the spectral ratio to a rock site: the 3 to 5Hz frequency components predominate at KOB, 2 to 4Hz at FKI, and 2Hz at FKE.

The boundaries of the layers have been divided into the boundary elements as tabulated in Tab.1. The total number of elements is 765(1,269 degrees of freedom). The response functions of the surface nodes have been estimated with frequencies upto 7 Hz. Fig.3 shows the surface displacements due to an incident Ricker wavelet with 1 Hz peak frequency(f_p). It can be found that the waveforms are characterized by the phases that propagate along the surface from the basin edge.

4.2 AVERAGE AMPLIFICATION FACTOR

4.2.1 COMPARISONS IN FREQUENCY AXIS

Fig.4(a) shows the average amplification factors at the KOB, FKI and FKE sites. At the KOB site, the average amplification factor is smaller than those at other two sites, and also flatter in shape. On the other hand, if we

Table 1: Summary of model parameters

Region	S wave velocity m/s	Density g/cm^3	Q	Number of elements (surface)	Length of elements m
1	2,850	2.2	∞	147(17)	19.6~29.4
2	1,100	2.0	150	207(0)	19.3~19.6
3	500	1.9	90	406(0)	10.0~19.3
4	300	1.8	60	502(251)	10.0

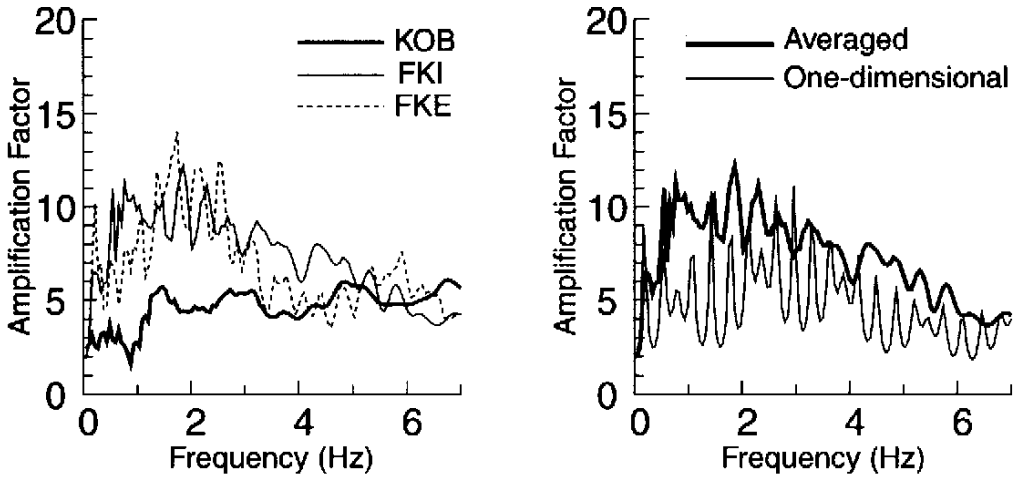

Figure 4: Comparisons of the amplification factors in a frquency axis

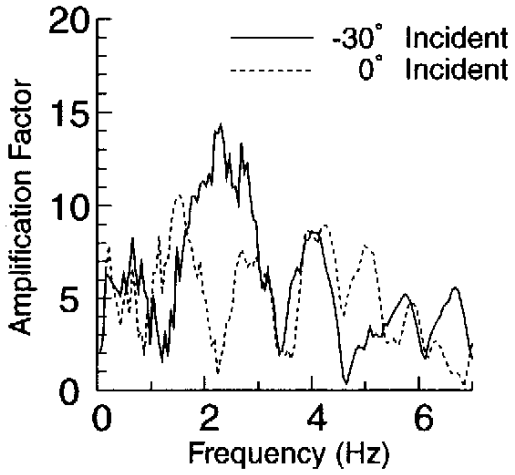

Figure 5: Comparison between the plane wave amplification factors with 0 and -30 degrees incident angles

disregard the ripples, both the peak about ten times at 2 Hz and the tendency to decrease with increasing frequency can be found with the average amplification factors at the FKI and FKE sites.

Fig.4(b) shows a comparison between the average and one-dimensional amplification factors at the FKI site. The latter have been estimated using the one-dimensional ground structure at the FKI site shown in Fig.2. From this comparison, it has been found that the one-dimensional amplification factor is smaller than the average amplification factor in the entire frequency range. Also it has been observed that the average amplification factor is more stable than the one-dimensional one, and the effects of the one-dimensional multiple reflection were involved in the average amplification factor from the fact that the frequencies which give the ripples on the average amplification factor are coincident with those of the one-dimensional one.

Fig.5 shows the plane wave amplification factors with 0 and -30 degrees incident angles. In the factor due to incidence with -30 degrees, the remarkable peak about fifteen times at 2.2 Hz has been observed, and considering the locations of the focal region and site, it can be concluded that this amplification can be related to the severely damaged band. However, the factor to the vertical incident is very small in this frequency range. From this comparison, it can be understood that one has to pay his attention to the sensitivity of the plane wave amplification to the incident angle.

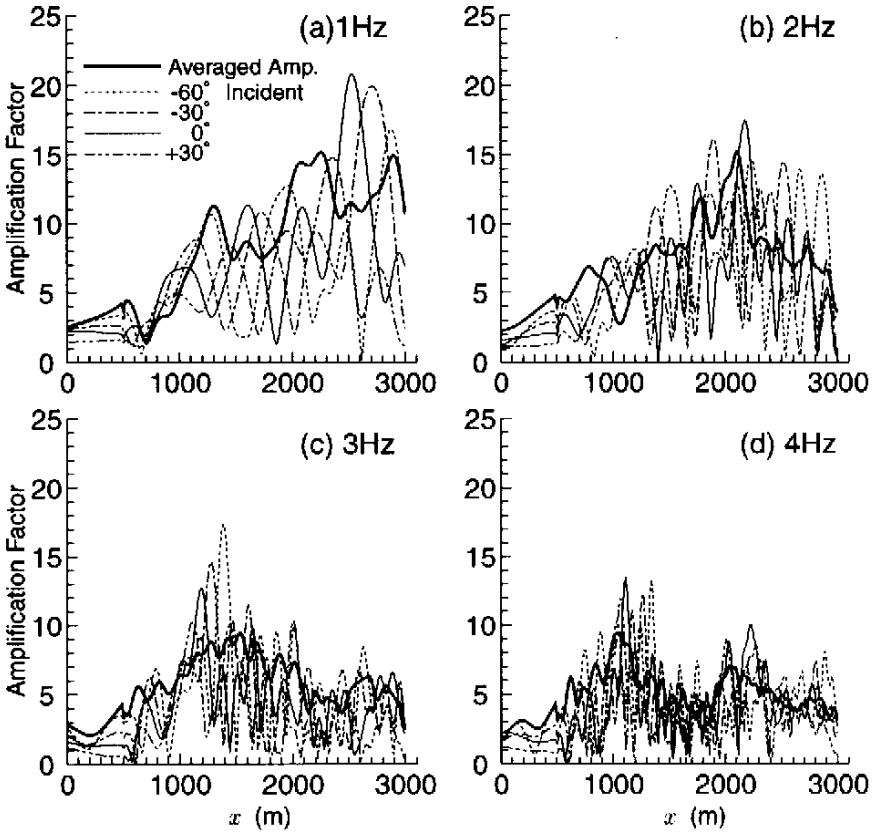

Figure 6: Comparisons between the distributions of the average and plane wave amplification factors along the ground surface x for 1, 2, 3 and 4 Hz

4.2.2 COMPARISONS IN SPACE AXIS

Figs.6(a) to (d) show comparisons between the distributions of the average and plane wave amplification factors for 1 to 4 Hz. The abscissa x is the distance measured along the ground surface. In these figures, the thick line indicates the average amplification factor.

From the comparisons of these figures, it can be observed that the locations where the peak amplification appears for the lower frequencies is farther from the basin edge than that for the higher frequencies. This can be understood as a constraint effect due to the existence of the bedrock near the surface. It can be said that when the basin edge is far, the lower the frequency becomes, the more the bedrock suppresses the surface motion because of the long wavelength.

The comparisons between the average and plane wave amplification factors show us the sensitivity of the plane wave amplification factors to the observational location in addition to the incident angle as mentioned before. Also as shown in the figures, it is obvious that this phenomenon becomes more remarkable with increasing frequency. Therefore, it should be noticed that whenever we examine the amplification effects by assuming an incident plane wave, we have to pay attention to this sensitivity.

On the contrary, the average amplification factors have the shapes approximately consistent with the envelope of the plane wave amplification factors except the sharp peaks around $x = 1,200$m for 3 and 4 Hz. From this property, the average amplification factor can be applied to examine the amplification characteristics of the ground in the case when the incident wave field is unpredictable. The sharp peaks in the plane wave amplification factors, as mentioned previously, are due to the high coherence of the incident wave because the abusolute values of the average coherence is unity for a plane wave. From these phenomena, the estimate of the coherence of the incident wave can be considered as an important theme in further studies on the amplification characteristics of the ground.

5. CONCLUSIONS

In this study, we have introduced both the average amplification factor and the average coherence, and applied them to the two-dimensional Kobe ground model. From these results, the followings have been pointed out.

1. At the FKI and FKE sites, the average amlification factors show the peak about 10 at 2 Hz, but at the KOB site, the clear peak cannot be found.
2. The amplification factors based on one-dimensional multiple reflections show sensitivity to changes of frequencies.
3. The amplification factor to a plane wave shows the sensitivity to the changes of the incident angle and location.
4. The average amplification factor cannot give the local amplification due to certain incident waves, however, it can give the stable values closed to an envelope of the plane wave amplifications.
5. Considering the mentioned above, it has been concluded that the average amplification factor can represent a measure of amplification effects of subsurface irregularities in the case when the incident wave field is unpredictable.

REFERENCES

Brebbia, C. A. and Walker, S. (1980), *Boundary element techniques in engineering*, Butterworth & Co. Ltd.

Hayashi, Y. and Kawase, H. (1996), "Strong motion evaluation in Chuo ward, Kobe, during the Hyogo-ken Nambu earthquake of 1995", *J. Struct. Constr. Eng., AIJ*, 481, pp37–46 (in Japanese).

Irikura, K. (1995), "Causative faults, strong ground motions and damages from the 1995 Hyogo-ken Nanbu earthquake", *BUTSURI–TANSA*, 48, 6, pp463–489 (in Japanese).

Iwata, T., Hatakeyama, K., Kawase, H. and Irikura, K. (1996), "Site amplification of ground motions during aftershocks of the 1995 hyogo-ken Nanbu earthquake in severely damaged zone — Array observation of ground motions in Higashi-Nada ward, Kobe city, Japan —", *J. Phys. Earth*, 44, pp553–561.

Kawase, H. and Hayashi, Y. (1996), "Strong motion simulation in Chuo ward, Kobe, during the Hyogo-ken Nambu earthquake of 1995 based on the inverted bedrock motion", *J. Struct. Constr. Eng., AIJ*, 480, pp67–76 (in Japanese).

Pitarka, A., Irukura, K., Iwata, T., and Kagawa, T. (1996), "Basin structure effects in the Kobe area inferred from the modeling of ground motions from two aftershocks of the January 17, 1995, Hyogo-ken Nanbu Earthquake", *J. Phys. Earth*, 44, pp563–576.